

Article

Hydrogen Desorption Properties of Bulk and Nanoconfined $\text{LiBH}_4\text{-NaAlH}_4$

Payam Javadian ^{1,2}, Drew A. Sheppard ², Craig E. Buckley ² and Torben R. Jensen ^{1,*}

¹ Center for Energy Materials, Interdisciplinary Nanoscience Center (iNANO), and Department of Chemistry, Aarhus University, DK-8000 Aarhus, Denmark; payam_javadian@hotmail.com

² Department of Imaging and Applied Physics, Curtin University, GPO Box U 1987, Perth, WA 6845, Australia; drew.sheppard@gmail.com (D.A.S.); C.Buckley@curtin.edu.au (C.E.B.)

* Corresponding: trj@chem.au.dk; Tel.: +45-87-155939 or +45-22-721486; Fax: +45-87-196199

Academic Editors: Umit B. Demirci, Philippe Miele and Pascal G. Yot

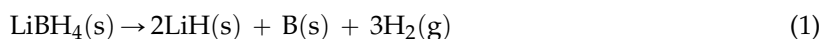
Received: 10 April 2016; Accepted: 9 June 2016; Published: 20 June 2016

Abstract: Nanoconfinement of $2\text{LiBH}_4\text{-NaAlH}_4$ into a mesoporous carbon aerogel scaffold with a pore size, BET surface area and total pore volume of $D_{\text{max}} = 30$ nm, $S_{\text{BET}} = 689$ m²/g and $V_{\text{tot}} = 1.21$ mL/g, respectively is investigated. Nanoconfinement of $2\text{LiBH}_4\text{-NaAlH}_4$ facilitates a reduction in the temperature of the hydrogen release by 132 °C, compared to that of bulk $2\text{LiBH}_4\text{-NaAlH}_4$ and the onset of hydrogen release is below 100 °C. The reversible hydrogen storage capacity is also significantly improved for the nanoconfined sample, maintaining 83% of the initial hydrogen content after three cycles compared to 47% for that of the bulk sample. During nanoconfinement, LiBH_4 and NaAlH_4 reacts to form LiAlH_4 and NaBH_4 and the final dehydrogenation products, obtained at 481 °C are LiH , LiAl , AlB_2 and Al . After rehydrogenation of the nanoconfined sample at $T = 400$ °C and $p(\text{H}_2) = 126$ bar, amorphous NaBH_4 is recovered along with unreacted LiH , AlB_2 and Al and suggests that NaBH_4 is the main compound that can reversibly release and uptake hydrogen.

Keywords: nanoconfinement; metal borohydride; sodium alanate

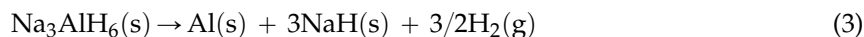
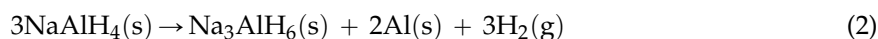
1. Introduction

Solid state hydrogen storage has received significant attention during the past few decades and is associated with a future carrier of renewable energy [1,2]. Initially, metal hydrides and magnesium hydride were the focus for much research and several useful applications have been developed [3–6]. In particular, lithium borohydride, LiBH_4 , is considered a potential candidate as a hydrogen storage material due to its relatively high gravimetric hydrogen storage capacity of $\rho_m = 13.6$ wt. % based on decomposition reaction (1) taking place above 375 °C in vacuum.

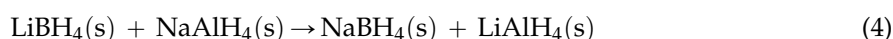


However, the kinetics for hydrogen release and uptake is very sluggish *i.e.*, hydrogen uptake requires elevated temperatures and pressures, $T = 600$ °C and $p(\text{H}_2) > 155$ bar [7]. One way to alter kinetic properties for hydrogen release of reactive composites of LiBH_4 is by additives using transition metals such as Ti, V, Cr or Sc [8–11]. Other metals like Al and Mg have also shown significant destabilization abilities as a reactive hydride composite (RHC) with LiBH_4 , by reducing the enthalpy of reversible dehydrogenation and rehydrogenation reactions [12–14]. Al nanoparticles have also been considered as an Al-source but the properties are generally inhibited due to an oxide layer, which limits the reactivity [10]. Another drawback for the $\text{LiBH}_4\text{-Al}$ system is the significant reduction of the hydrogen content, which has pointed attention towards NaAlH_4 as the Al source. Furthermore,

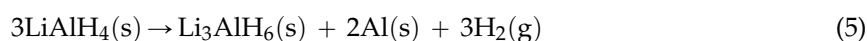
NaAlH₄ can reversibly store hydrogen at moderate conditions according to the two-step decomposition reaction shown in reactions (2) and (3).



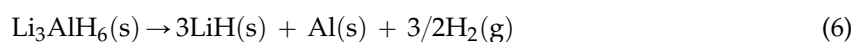
The hydrogen storage capacity associated with the two-step reaction is $\rho_m = 5.6$ wt. % [15,16]. Mixed hydride systems have previously been studied in various ratios, *i.e.*, LiBH₄-NaAlH₄, 2LiBH₄-NaAlH₄ and 2LiBH₄-3NaAlH₄ [17], and with selected Ti-based additives [18]. Different reaction pathways may occur, depending on the composition as shown in reactions (4) and (5).



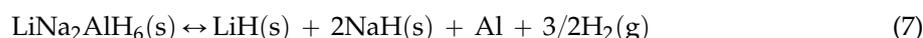
where LiAlH₄ also release hydrogen in two steps according to reactions (5) and (6)



Above 100 °C, without doping, Li₃AlH₆ reacts to release hydrogen according to reaction (6)



Furthermore, it is found that with excess NaAlH₄ in the 2LiBH₄-3NaAlH₄ system, the decomposition product NaH reacts reversibly forming LiNa₂AlH₆ at $T = 180$ °C and $p(\text{H}_2) = 80$ bar [18] according to reaction (7):



In the case of excess LiBH₄ (2LiBH₄-NaAlH₄), mixed phases of NaBH₄ and LiAlH₄ are formed. However, during dehydrogenation AlB_x, Al_{1-x}Li_xB₂ and LiAl were observed at 425 and 450 °C, respectively [17].

Nanoconfinement of metal hydrides may change the reaction mechanism for reactive hydride composites, and may also improve the kinetics for chemical reactions significantly [19–21]. Confinement of NaAlH₄ in carbon aerogel, which was also activated or functionalized, has been investigated. The fastest kinetics are observed for TiCl₃ functionalized scaffolds, while CO₂ activated scaffolds provide slower kinetics but more efficient infiltration and higher reversible hydrogen storage capacity over several cycles of hydrogen release and uptake [22–24].

This work presents hydrogen release and uptake properties of nanoconfined 2LiBH₄-NaAlH₄ into a nanoporous carbon aerogel scaffold, synthesised via melt infiltration for further improvement of the system, with the purpose of destabilizing the borohydride in the solid state. Various techniques are used to investigate hydrogen storage properties of this system.

2. Experimental Details

2.1. Sample Preparation

The resorcinol formaldehyde carbon aerogel was prepared by mixing 82.87 g resorcinol (Aldrich, 99%), 113.84 mL formaldehyde (37 wt. % stabilized by ~10%–15% methanol, Merck), 113.28 mL deionized water and 0.0674 g Na₂CO₃ (Aldrich, 99.999%) in a beaker with continuous stirring until complete dissolution was obtained. The pH of the final solution was measured to be 5.91. The preparation and characterization of the aerogel was performed according to previously published procedures [22,25,26]. Prior to use, the scaffolds were all degassed at 400 °C in a dynamic vacuum for several hours, in order to remove possible adsorbed air and water confined inside the porous structure.

This carbon aerogel scaffold is denoted CA. All subsequent handling was performed in a glovebox with a purified argon atmosphere.

Commercially available NaAlH_4 (Aldrich, 93%) was physically mixed with LiBH_4 (Aldrich, $\geq 95.0\%$) in the molar ratio $2\text{LiBH}_4\text{-NaAlH}_4$ which was recently reported to show suitable melt infiltration abilities [27]. This sample is denoted LiNa.

An amount of hydride was selected in order to obtain ~ 33 vol. % pore filling of the carbon scaffold based on the total pore volume, V_{tot} , of the scaffold and the average bulk densities of the hydrides, $\rho(\text{LiNa}) = 0.8482$ g/mL. Melt infiltration was performed in a custom made rig, by heating to $T = 310$ °C ($\Delta T/\Delta t = 2$ °C/min) with the temperature kept fixed at 310 °C for 30 min, at a hydrogen pressure of 110 bar. Afterwards the sample was cooled naturally to room temperature (RT).

2.2. Sample Characterization

Synchrotron radiation powder X-ray diffraction (SR-PXD) data was collected at beamline I711 at MAX-lab, Lund, Sweden. The samples were mounted in a sapphire capillary tube (0.79 mm I.D.), in an airtight sample holder inside an argon filled glovebox [28,29]. The sample holder was removed from the glovebox and attached to a gas control system at the synchrotron diffractometer. The data was collected using a MAR165 CCD detector with a selected wavelength of $\lambda = 0.991779$ Å. Heating was applied by a tungsten wire placed under the capillary, whereas the temperature was controlled by an external PID regulator and thermocouple inserted into the powder-bed as previously shown [28].

A Perkin Elmer STA 6000 was utilized to conduct thermogravimetric analysis (TGA) coupled with a Hiden Analytical quadrupole mass spectrometer (MS) for differential scanning calorimetry (DSC). Thus, temperature-programmed desorption mass spectroscopy (TPD-MS) data is provided. Data was collected with a constant flow (64 mL/min) of argon (99.99%). A powdered sample (< 5 mg), was placed in an Al_2O_3 crucible with lid and heated in the temperature range of 40 to 550 °C ($\Delta T/\Delta t = 10$ °C/min). The MS signals at $m/e = 2, 18$ and 34 were recorded in order to detect H_2 , H_2O and B_2H_6 .

The reversible hydrogen storage capacity of nanoconfined and bulk $2\text{LiBH}_4\text{-NaAlH}_4$ was studied during multiple hydrogen release and uptake cycles. The samples were sealed in an autoclave under argon and attached to the Sieverts' apparatus (PCTpro 2000). Hydrogen desorption data was collected starting under an initial H_2 pressure of 1 bar and was performed in the temperature range of RT to 500 °C, ($\Delta T/\Delta t = 5$ °C/min), with the temperature kept constant at 500 °C for 10 h. Hydrogen absorption was performed in the pressure range of $p(\text{H}_2) = 140$ to 150 bar, at a temperature of 400 °C ($\Delta T/\Delta t = 5$ °C/min) during 10 h, and then the sample was cooled naturally to RT.

The Fourier transform infrared spectrometry (FTIR) analyses were carried out on a NICOLET 380 FT-IR from Thermo-Electronic Corporation with permanently aligned optics and proprietary diamond-turned pinned-in-place mirror optics. A small amount of sample was placed on the baseplate and subsequently the diamond pin was pressed on to the sample, forming a thin film. The samples were examined within the wave number range of 400–4000 cm^{-1} . The samples were briefly exposed to air when mounted in the instrument.

3. Results and Discussion

3.1. In Situ Synchrotron Radiation—Powder X-Ray Diffraction of Bulk and Nanoconfined $2\text{LiBH}_4\text{-NaAlH}_4$

The decomposition of physically mixed bulk $2\text{LiBH}_4\text{-NaAlH}_4$ (LiNa) has been investigated using *in situ* SR-PXD during heating up to 487 °C, see Figure 1. At RT a physical mixture of the low temperature polymorph orthorhombic LiBH_4 , *o*- LiBH_4 , and NaAlH_4 are present in the sample. The polymorphic transition from *o*- LiBH_4 to hexagonal *h*- LiBH_4 takes place in the temperature range 98 to 105 °C. A metathesis reaction between LiBH_4 and NaAlH_4 occurs at 116 °C observed by formation of NaBH_4 . This may be the metathesis reaction described by reaction (4), however LiAlH_4 is not observed. Lithium tetrahydridoaluminate, LiAlH_4 , may decompose immediately according to reaction (5), which explains observation of Li_3AlH_6 in the temperature range 116 to 227 °C. Since diffraction from

Na_3AlH_6 and NaH is not observed, NaAlH_4 is expected to be fully converted by the metathesis reaction (4) rather than decomposition via reactions (2) and (3). Characteristic strong diffraction at $2\theta = 25^\circ$ and 28° from Al occur at $T = 115^\circ\text{C}$ and is assumed mainly to be formed via the decomposition of LiAlH_4 . Similarly, diffraction from $h\text{-LiBH}_4$ is not visible in the data possibly due to reaction (4). NaBH_4 is observed in the temperature range from 116 to 435°C . Weak diffraction from LiH , is also observed in the temperature range 116 and 485°C , partially overlapping with the Al peaks and is expected mainly to be formed by decomposition of Li_3AlH_6 . Furthermore, two unknown peaks are observed at $2\theta \sim 20^\circ$ and $2\theta \sim 23^\circ$, forming simultaneous to Li_3AlH_6 . A shift of Bragg peaks towards smaller 2θ angles is observed due to thermal expansion and the associated increase in unit cell parameters. During natural cooling of the sample, thermal contraction is observed along with formation of Al , LiAl_3 , and NaBH_4 along with an unknown compound. A difference plot of the *in situ* SR-PXD data is shown in supporting information to accentuate changes in weaker peaks.

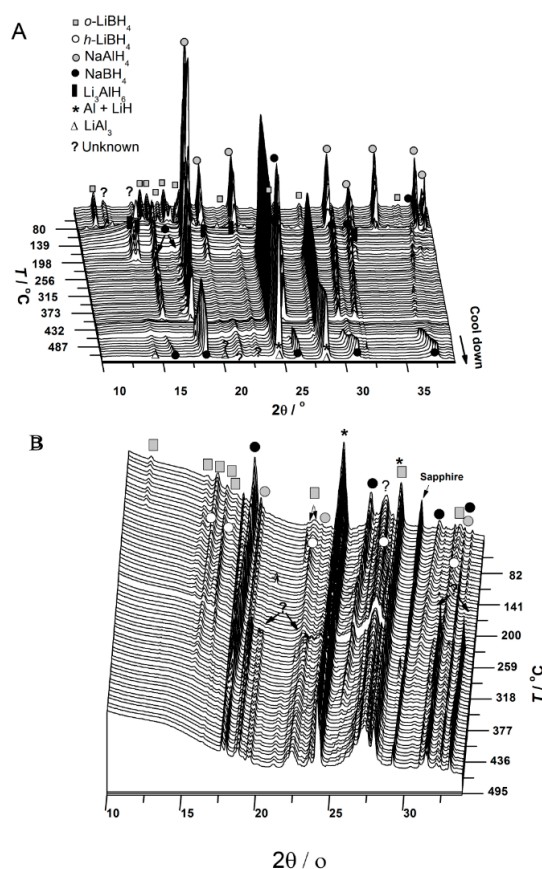
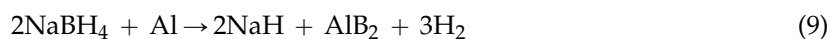


Figure 1. *In situ* SR-PXD during dehydrogenation of (A) bulk $2\text{LiBH}_4\text{-NaAlH}_4$ heated from room temperature (RT) to 487°C , with subsequent natural cooling to RT in $p(\text{H}_2) = 1$ bar and (B) nanoconfined $2\text{LiBH}_4\text{-NaAlH}_4$ in carbon aerogel (CA) heated from RT to 495°C ($\Delta T/\Delta t = 5^\circ\text{C}/\text{min}$, $\lambda = 0.991779 \text{ \AA}$).

A decrease in the background scattering occurs between 160 and 198°C which coincides with the maximum rate of Li_3AlH_6 and Al formation. Further work would be required to determine if this relationship is causative or correlative. The Li_3AlH_6 diffraction decreases at $T > 192^\circ\text{C}$ and disappears at $T \sim 227^\circ\text{C}$. The decomposition of Li_3AlH_6 is associated with further production of Al and the observation of weak diffraction from LiH . Following decomposition reactions could take place:





Diffraction of NaBH_4 decreases in intensity at 412 to 435 °C just prior to a slight increase in the background intensity. Weak peaks of an unknown compound at $2\theta \sim 14^\circ$, $\sim 21^\circ$ and $\sim 22^\circ$ are also observed to form simultaneously. It should be noted that the disappearance of NaBH_4 at 435 °C occurs well below both its melting point of 505 °C and the decomposition temperature of $T(1 \text{ bar}) \sim 515\text{--}534$ °C [30]. The simultaneous decrease in diffracted intensity of LiH and NaBH_4 may suggest eutectic melting supported by the reappearance of NaBH_4 and LiH upon cooling at 487 °C. We note that eutectic melting of $\text{NaBH}_4\text{-NaH}$ at $T = 395$ °C has previously been observed [31].

In situ SR-PXD of nanoconfined $\text{LiBH}_4\text{-NaAlH}_4$ measured during heating to 495 °C is shown in Figure 1. At RT diffraction of LiBH_4 and small amounts of NaAlH_4 are observed and partial decomposition due to the temperature used for the melt infiltration would explain the presence of diffraction peaks assigned to Al. Furthermore, the presence of NaBH_4 at RT also indicates metathesis reaction (4) during melt infiltration. A broad unknown peak at $2\theta = 27^\circ$ is observed throughout the measurement. The *o*- LiBH_4 to *h*- LiBH_4 polymorphic transition is observed, however only during a short temperature range of 97 to 110 °C. The background intensity decrease in the temperature range $T \sim 238$ to 250 °C but is most pronounced below $2\theta = 15^\circ$ and is associated with the formation of two peaks from an unknown phase at $2\theta \sim 19^\circ$ and $2\theta \sim 23^\circ$. These peaks are similar to those formed in the bulk sample. At $T = 318$ °C, a diffraction peak appears at $2\theta \sim 21.3^\circ$ which coincides with a decrease in diffraction intensity from NaBH_4 . This peak continues to slowly grow until all of the NaBH_4 decomposes at $T \sim 406$ °C. At ~ 487 °C, unknown peaks begin to form at $2\theta \sim 19^\circ$, 22° and 31.4° and these slowly grow until the heating stops. The growth of these peaks is associated with a slight decrease in the intensity of the Al peaks. The unknown peaks may result from a reaction between the hydride(s) and possible oxygen impurities in the aerogel scaffold. However, due to the relatively weak and overlapping Bragg reflections, indexation remain unsuccessful.

3.2. Nanoporous Carbon Aerogel Composite

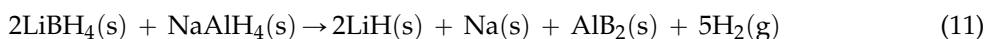
The synthesized resorcinol formaldehyde carbon aerogel (CA) scaffold has a maximum pore size distribution centred on $D_{\text{max}} = 30$ nm, a specific BET surface area of $S_{\text{BET}} = 689 \text{ m}^2/\text{g}$ and a total pore volume of $V_{\text{tot}} = 1.21 \text{ mL/g}$ (see Table 1).

Table 1. Texture parameters of as prepared carbon aerogel scaffold (CA). The gravimetric hydrogen content of the confined sample is also provided.

Scaffold	S_{BET} (m^2/g)	V_{micro} (mL/g)	V_{meso} (mL/g)	V_{tot} (mL/g)	D_{max} (nm)	LiNa* (wt. %)	Theoretical H_2 Content (wt. %) [#]
CA	689 ± 26	0.21 ± 0.02	1.06 ± 0.10	1.21 ± 0.10	30 ± 0.15	-	-
CA-LiNa	257 ± 26	0.06 ± 0.02	0.71 ± 0.10	0.78 ± 0.10	21 ± 0.15	25.3	2.6

* Amount of $2\text{LiBH}_4\text{-NaAlH}_4$ used for the infiltration per weight and volume of the scaffold; [#] Prior to melt infiltration.

The binary hydride composite $2\text{LiBH}_4\text{-NaAlH}_4$ (LiNa) has been successfully melt infiltrated into the mesoporous carbon scaffold via melt infiltration upon elevated hydrogen pressures of $p(\text{H}_2) = 110$ bar, in order to avoid decomposition of the respective hydrides (please see note about this in experimental section). Confinement of the hydride mixture facilitates the formation of nanoparticles of the respective hydrides, in accordance with previous studies [27]. The amount of $2\text{LiBH}_4\text{-NaAlH}_4$ added to CA is 25.3 wt. % corresponding to 33 vol. % pore filling. The theoretical hydrogen content of the binary hydride system is $\rho_{\text{m}}(\text{LiNa}) = 10.33$ wt. % calculated using the bulk densities of the respective hydride according to the molar ratios and reaction (11)



The available hydrogen capacity of the CA-LiNa confined sample is determined to be 2.6 wt. % H₂. However, considering 100 vol. % pore filling would potentially give a 7.8 wt. % hydrogen capacity.

3.3. Decomposition of Bulk and Nanocomposites of 2LiBH₄-NaAlH₄

The of hydrogen desorption from bulk 2LiBH₄-NaAlH₄ (LiNa), LiNa physically mixed with carbon aerogel scaffold (CA) and LiNa melt infiltrated into CA, was analysed by TG-DSC-MS during heating from 40 to 550 °C with the results shown in Figure 2. The TG-DSC-MS measurements can provide information about the endothermic and exothermic nature of any transitions or chemical reactions that take place during heating. In addition, if the same transitions and chemical reactions occur in different samples, TG-DSC-MS can provide information about the relative kinetic differences between samples. Each data set is normalized to the maximum hydrogen desorption rate to allow for qualitative comparison between data sets. Hydrogen emission from bulk 2LiBH₄-NaAlH₄ is observed as two local maxima at 234 and 496 °C. The first hydrogen release peak in the MS spectrum ($T = 200\text{--}250\text{ °C}$) is associated with the decomposition of Li₃AlH₆ in accord with the *in situ* SR-PXD data (see Figure 1). This temperature range is in good agreement with previous reports on decomposition of bulk Li₃AlH₆ (180–230 °C) [32,33]. A mass loss of 3.36 wt. % is observed by TGA in the temperature range 200 to 250 °C. Differential scanning calorimetry data reveal two thermal events at 112 and 120 °C, which may be assigned to the polymorphic *o*- to *h*-LiBH₄ transition and the metathesis reaction (reaction 4), respectively. Partial amorphisation or melting of the sample may occur, which may be observed as a significant increase in the background of the diffraction data in the temperature range 70 to 150 °C (see Figure 1). Several thermal events in the temperature range ~200 to 220 °C may be associated with partial melting of the sample and decomposition of Li₃AlH₆ [32]. Eutectic melting of the LiBH₄-NaBH₄ is reported to occur at ~250 °C without release of hydrogen [30].

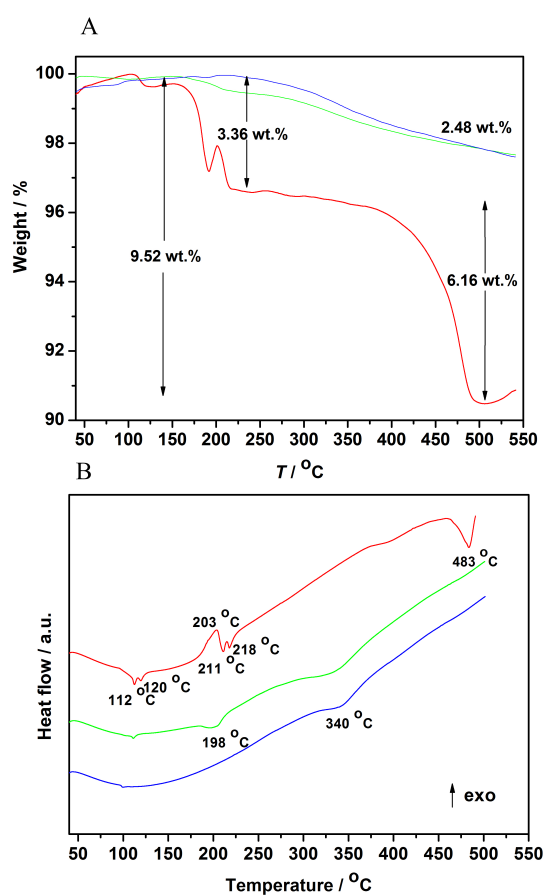


Figure 2. Cont.

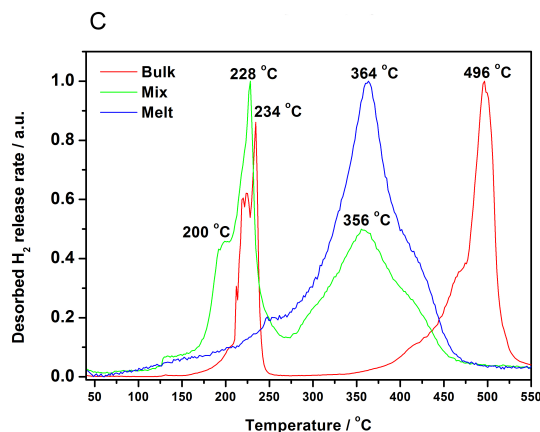


Figure 2. (A) Thermal programmed desorption mass spectroscopy (TPD-MS) profiles of the hydrogen release (H_2^+ ions, $m/e = 2$); (B) thermogravimetric analysis (TGA); and (C) differential scanning calorimetry (DSC) measurements of bulk $2\text{LiBH}_4\text{-NaAlH}_4$ (LiNa) (red), LiNa mixed with carbon aerogel scaffold (CA) (green) and LiNa melt infiltrated into CA (blue). The data is measured in the temperature range 40 to 550 °C and TPD-MS for each data set is normalized by its maximum hydrogen release rate to allow for qualitative comparison ($\Delta T/\Delta t = 10$ °C/min).

The second MS hydrogen release event ($T = 350\text{--}500$ °C) of bulk LiNa is assigned to the decomposition of remaining LiBH_4 and NaBH_4 , which corresponds to a weight loss of 6.16 wt. %. The total TGA mass loss in the temperature range 40 to 550 °C is 9.52 wt. %, which corresponds to 92% of the available hydrogen content ($\rho_m(\text{LiNa}) = 10.33$ wt. %).

The carbon containing samples (physically mixed and melt infiltrated) both release 2.48 wt. % H_2 when heated from 40 to 550 °C, which corresponds to 95% of the theoretical hydrogen content in the sample (see Figure 2). However, the physically mixed sample has a hydrogen release profile similar to that of bulk LiNa at $T < \sim 250$ °C with a peak value at $T = 228$ °C shifted 6 °C towards lower temperatures. The nanoconfined sample LiNa-CA does not show the aforementioned desorption peak. The temperature of the maximum hydrogen release rate of the mixed ($T = 356$ °C) and melt infiltrated samples ($T = 364$ °C) occur at significantly reduced temperatures ($\Delta T \sim 130$ °C) as compared to that of bulk $\text{LiBH}_4\text{-NaAlH}_4$ ($T = 496$ °C). This effect has previously been reported for other nanoconfined binary hydride systems that showed a reduction in the temperature of the maximum hydrogen release rate compared to bulk, e.g., $\text{LiBH}_4\text{-Mg}(\text{BH}_4)_2$ ($\Delta T_{\text{max}} \sim -60$ °C), $\text{LiBH}_4\text{-Ca}(\text{BH}_4)_2$ ($\Delta T_{\text{max}} \sim -95$ °C) and $\text{LiBH}_4\text{-NaBH}_4$ ($\Delta T_{\text{max}} \sim -107$ °C) [33–35].

The improvement of hydrogen release kinetics due to the carbon scaffold, is assigned to the effect induced by nanoconfinement and possible catalytic properties of the carbon surface [36]. In addition, the DSC signal assigned to the major hydrogen desorption at $T \sim 340$ °C is reduced by ~ 140 °C as compared to that of bulk LiNa.

According to Figure S2, after decomposition of the nanoconfined sample AlB_2 , LiAl_3 , LiH and some unknown phases are formed. No diffraction Bragg peaks of NaBH_4 are displayed suggesting possible formation of amorphous metal borides. This is supported by the FTIR data discussed later.

3.4. Cyclic Stability

The reversible hydrogen storage properties of bulk and nanoconfined $2\text{LiBH}_4\text{-NaAlH}_4$ (LiNa) have been investigated by the Sieverts' method during multiple hydrogen release and uptake cycles and the data is displayed in Figure 3. During heating of bulk LiNa from RT to 500 °C, hydrogen is released in two steps with a plateau of slow hydrogen evolution in the temperature range 160 to 190 °C. The total amount of hydrogen released from the sample during the first desorption in the temperature range RT to 500 °C is 8.37 wt. %, which is 81% of the theoretical available hydrogen content. After subsequent rehydrogenation at $p(\text{H}_2) = 126$ bar, $T = 400$ °C for 10 h, the second, third and

fourth desorption cycle release 4.65, 3.94 and 3.38 wt. % H_2 , corresponding to 56%, 47% and 40% of the initial hydrogen content, respectively. The slow hydrogen release at 160 to 190 °C is only observed during the first desorption, as clearly demonstrated in Figure 4. Thus, the reversible fraction of the sample may be $LiBH_4$ and/or $NaBH_4$ formed in a possibly amorphous form. Sodium and lithium alanate are not expected to form at the high temperatures used for rehydrogenation. This fact along with the formation of stable decomposition products LiH , $LiAl_3$ and Al , may explain the significant difference between the hydrogen storage capacities observed after the first desorption.

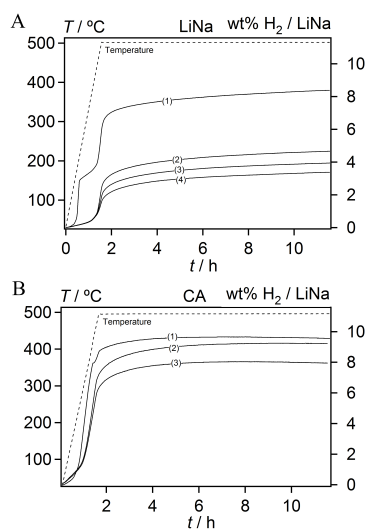


Figure 3. Sieverts' measurement showing four and three hydrogen release cycles for (A) bulk $2LiBH_4-NaAlH_4$ and (B) infiltrated into CA, $LiNa-CA$. Hydrogen desorption was performed at a fixed temperature of 500 °C ($\Delta T/\Delta t = 5$ °C) for 10 h under an initial hydrogen pressure of 1 bar. Hydrogen absorption was performed at 400 °C, $p(H_2) = 126$ bar for 10 h.

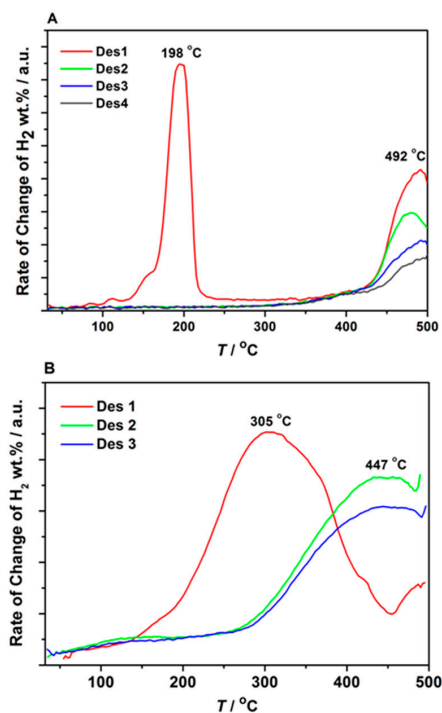


Figure 4. Differentiated Sieverts' data for four and three desorption cycles of (A) bulk $2LiBH_4-NaAlH_4$ and (B) nanoconfined $2LiBH_4-NaAlH_4$ in CA.

The nanoconfined sample, LiNa-CA, showed substantially improved cyclic stability and improved hydrogen storage capacity compared to that of bulk LiNa as shown in Figure 3. The hydrogen release of LiNa-CA is shown relative to the amount of $2\text{LiBH}_4\text{-NaAlH}_4$ in the nanoconfined to facilitate comparison with LiNa. The hydrogen release from the nanoconfined system also has a two-step behaviour for the first H_2 desorption profile similar to bulk LiNa but at higher temperatures ($\sim 380^\circ\text{C}$). The first desorption of LiNa-CA releases 9.6 wt. % H_2 with respect to LiNa and 2.4 wt. % relative to the total mass of the sample. This corresponds to 93% of the theoretical available hydrogen content ($\rho_m(\text{LiNa-CA}) = 2.6$ wt. % H_2). It is worth noting that the nanoconfined sample is fully desorbed after 2 h at 500°C , whereas bulk $2\text{LiBH}_4\text{-NaAlH}_4$, on the contrary continues to release hydrogen throughout the entire measurement. The second and third desorptions release 9.2 and 7.9 wt. % H_2/LiNa corresponding to 96% and 83% of the initial hydrogen content, and equivalent to 89% and 77% of the available hydrogen content, respectively. These results demonstrate that nanoconfinement has significantly improved hydrogen release kinetics and cyclic stability compared to bulk $2\text{LiBH}_4\text{-NaAlH}_4$.

Differentiated Sieverts' data provides the change in rate of H_2 release during each desorption cycle upon heating from RT to 500°C (see Figure 4). Selected desorption profiles from Figure 4 resemble the TPD-MS data shown in Figure 2, despite different measurement conditions and heating rates. During the first hydrogen release cycle of bulk LiNa, the maximum H_2 release rate is observed at 198°C which corresponds to the first plateau observed in Figure 3. A second peak value at 492°C is in good agreement with TPD-MS measurements in Figure 3. During the second, third and fourth desorption, only one hydrogen release event is observed with onset at $T \sim 440^\circ\text{C}$, which decreases in intensity with increasing desorption cycles.

The major hydrogen release of the nanoconfined sample (Figure 4B) is exhibited as a broad peak with maxima at 305°C during the first desorption. However during the second and third desorption an event is observed with a local maxima at 447°C . The lack of exothermic signal in the DSC measurement suggests that this hydrogen release is not due to a one-time irreversible reaction with oxygen impurities in the carbon framework. Instead it suggests that the hydrogen pressure applied at the temperature used for rehydriding was insufficient to fully reverse all of the hydrogen desorption reactions. *In situ* SR-PXD of the nanoconfined sample suggests that the first hydrogen release event on the first desorption cycle is due to residual unreacted LiBH_4 from incomplete metathesis (reaction 4). Once the remaining LiBH_4 has decomposed, it is not reformed under the applied hydriding conditions, thus it is not observed during the second desorption. Based on the *in situ* SR-PXD on the bulk sample, the compounds that are not regenerated under the applied temperatures and hydrogen pressures are possibly LiAlH_4 and/or Li_3AlH_6 [37].

FT-IR measurements on selected samples are presented in Figure 5. Bulk $2\text{LiBH}_4\text{-NaAlH}_4$ demonstrates multiple peaks in the fingerprint region ($500\text{--}1500\text{ cm}^{-1}$). The three signals at 1095 , 1241 and 1315 cm^{-1} , corresponds to the characteristic B-H bending bands of LiBH_4 . The signal at 1626 cm^{-1} is assigned to the $[\text{AlH}_4]^-$ stretching band of NaAlH_4 and the large broad signal ranging from 2000 to 2500 cm^{-1} , with a maximum at 2307 cm^{-1} , originates from the B-H stretch of LiBH_4 . Furthermore, the small signal at 3444 cm^{-1} , is assigned to $-\text{OH}$, most likely from exposure to atmospheric moisture moist during measurement. It is worth noting that moisture and air cannot be completely avoided during collection of FT-IR data using the selected apparatus. A completely dehydrogenated sample of melt infiltrated $2\text{LiBH}_4\text{-NaAlH}_4$ in CA, *i.e.*, heated at 500°C for 10 h shows a distinct signals at 1100 and 2462 cm^{-1} . These positions are close to those reported for $\text{Li}_2\text{B}_{12}\text{H}_{12}$ [38] and are nearly identical to positions reported by Mao *et al.* [39] after the decomposition of NaBH_4 which suggests that one of the decomposition products may be $\text{Na}_2\text{B}_{12}\text{H}_{12}$. Rehydrogenation of the decomposed sample after three desorption cycles at 400°C for 10 h, show B-H stretching signals at 2113 and 2283 cm^{-1} and the respective B-H bending. Furthermore, signals at 1234 and 1080 cm^{-1} are observed in the fingerprint region. These results may suggest that the 1234 and 2283 can be assigned to NaBH_4 in combination with another unknown complex boron hydride. It is difficult to make any statement about the possible presence of NaAlH_4 signals due to the high amount of carbon and low total quantity of hydrides in

the sample. Based on these results it can be suggested that the partial reversibility of the system is due to the formation and decomposition of NaBH_4 inside the scaffold.

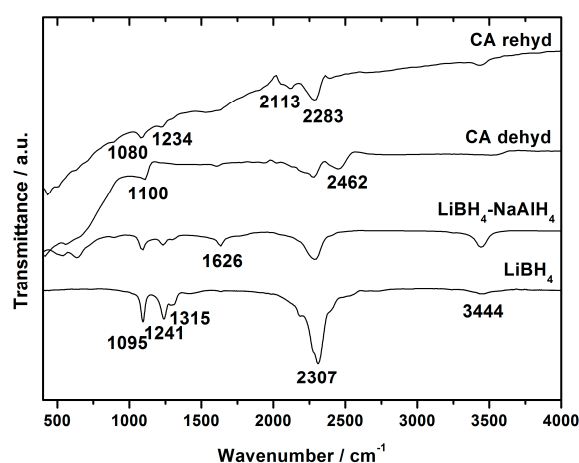


Figure 5. FTIR spectra of bulk LiBH_4 , $2\text{LiBH}_4\text{-NaAlH}_4$ (LiNa), and nanoconfined $2\text{LiBH}_4\text{-NaAlH}_4$ CA-LiNa after dehydrogenation at $500\text{ }^\circ\text{C}$ for the third time and finally CA-LiNa rehydrogenated at $p(\text{H}_2) = 140\text{ bar}$, $T = 400\text{ }^\circ\text{C}$ for 10 h after three desorption cycles. The intensity of the spectra with the carbon containing samples was scaled corresponding to their quantity of LiNa to allow for better comparison.

Fu *et al.* [40] reports elemental analysis of carbon aerogel prepared using alternative reagents but similar pyrolysis conditions. Analysis of carbon and oxygen concentration of the carbon aerogels after pyrolysis reveal C and O are 94.00 wt. % and 5.87 wt. %, respectively (re-calculated by excluding K). Assuming similar oxygen levels in our scaffolds and a 1:1 reaction with LiH would reduce the released amount of hydrogen to 2.066 wt. % H_2 for the nanoconfined sample.

4. Conclusions

Nanoconfinement of $2\text{LiBH}_4\text{-NaAlH}_4$ was obtained via melt infiltration under H_2 pressure and the reversibility and the reaction mechanisms during infiltration and decomposition are investigated. Nanoconfinement of $2\text{LiBH}_4\text{-NaAlH}_4$ into a mesoporous carbon aerogel scaffold significantly enhances the kinetics for hydrogen desorption, the hydrogen storage capacity and reversibility during hydrogen release and uptake cycling of $2\text{LiBH}_4\text{-NaAlH}_4$, compared to that of bulk. The temperature of the maximum hydrogen desorption rate is reduced by $132\text{ }^\circ\text{C}$ when employing the carbon scaffold, which is assigned to the effect induced by nanoconfinement and the carbon surface acting as a catalyst for hydrogen release on $2\text{LiBH}_4\text{-NaAlH}_4$. The stability during cycling is significantly enhanced by melt infiltration of the hydride. Bulk $2\text{LiBH}_4\text{-NaAlH}_4$ releases 81% of the available hydrogen content during the first desorption, compared to 96% when nanoconfined. During the third desorption cycle of the bulk sample, only 47% of the initial hydrogen content is retained compared to 83% for that of the nanoconfined sample. These results demonstrate significant stabilization of the cyclic hydrogen storage capacity of metal borohydrides compared to those previously presented.

Acknowledgments: The work was supported by the Innovation Fund Denmark (project HyFill-Fast), and by the Danish Research Council for Nature and Universe (Dancatt), the Danish National Research Foundation, Center for Materials Crystallography (DNRF93). Torben R. Jensen is grateful to the Carlsberg Foundation. Craig E. Buckley, Drew A. Sheppard and Payam Javadian acknowledge the financial support of the Australian Research Council (ARC) for ARC Linkage Grant LP120100435.

Author Contributions: Payam Javadian prepared the samples, obtained the experimental results and conducted the characterization experiments in collaboration with Drew A. Sheppard. All authors contributed to data analysis and to writing of the manuscript.

Conflicts of Interest: The authors declare no conflict of interest.

References

1. Ley, M.B.; Jepsen, L.H.; Lee, Y.S.; Cho, Y.W.; von Colbe, J.M.B.; Dornheim, M.; Rokni, M.; Jensen, J.O.; Sloth, M.; Filinchuk, Y.; *et al.* Complex hydrides for hydrogen storage—New perspectives. *Mater. Today* **2014**, *17*, 122–128. [[CrossRef](#)]
2. Callini, E.; Atakli, Z.Ö.K.; Hauback, B.C.; Orimo, S.-I.; Jensen, C.; Dornheim, M.; Grant, D.; Cho, Y.W.; Chen, P.; Hjörvarsson, B.; *et al.* Complex and liquid hydrides for energy storage. *Appl. Phys. A* **2016**, *122*, 1–22. [[CrossRef](#)]
3. Crivello, J.C.; Denys, R.V.; Dornheim, M.; Felderhoff, M.; Grant, D.M.; Huot, J.; Jensen, T.R.; de Jongh, P.; Latroche, M.; Walker, G.S.; *et al.* Mg-based compounds for hydrogen and energy storage. *Appl. Phys. A* **2016**, *122*, 1–17. [[CrossRef](#)]
4. Crivello, J.C.; Dam, B.; Denys, R.V.; Dornheim, M.; Grant, D.M.; Huot, J.; Jensen, T.R.; de Jongh, P.; Latroche, M.; Milanese, C.; *et al.* Review of magnesium hydride-based materials: Development and optimisation. *Appl. Phys. A* **2016**, *122*, 1–20. [[CrossRef](#)]
5. Yartys, V.; Noreus, D.; Latroche, M. Metal hydrides as negative electrode materials for Ni-MH batteries. *Appl. Phys. A* **2016**, *122*, 1–11. [[CrossRef](#)]
6. Lototsky, M.V.; Yartys, V.A.; Pollet, B.G.; Bowman, R.C. Metal hydride hydrogen compressors: A review. *Int. J. Hydrog. Energy* **2014**, *39*, 5818–5851. [[CrossRef](#)]
7. Zuttel, A.; Wenger, P.; Rentsch, S.; Sudan, P.; Mauron, P.; Emmenegger, C. LiBH₄ a new hydrogen storage material. *J. Power Sour.* **2003**, *118*, 1–7. [[CrossRef](#)]
8. Yang, J.; Sudik, A.; Wolverton, C. Destabilizing LiBH₄ with a metal (M = Mg, Al, Ti, V, Cr, or Sc) or metal hydride (MH₂, MgH₂, TiH₂, or CaH₂). *J. Phys. Chem. C* **2007**, *111*, 19134–19140. [[CrossRef](#)]
9. Yu, X.B.; Grant, D.A.; Walker, G.S. Low-temperature dehydrogenation of LiBH₄ through destabilization with TiO₂. *J. Phys. Chem. C* **2008**, *112*, 11059–11062. [[CrossRef](#)]
10. Meggouh, M.; Grant, D.M.; Walker, G.S. Optimizing the destabilization of LiBH₄ for hydrogen storage and the effect of different Al sources. *J. Phys. Chem. C* **2011**, *115*, 22054–22061. [[CrossRef](#)]
11. Purewal, J.; Hwang, S.J.; Bowman, R.C.; Ronnebro, E.; Fultz, B.; Ahn, C. Hydrogen sorption behavior of the ScH₂-LiBH₄ system: Experimental assesment of chemical destabilization effects. *J. Phys. Chem. C* **2008**, *112*, 8481–8485. [[CrossRef](#)]
12. Ravnsbaek, D.B.; Jensen, T.R. Mechanism for reversible hydrogen storage in LiBH₄-Al. *J. Appl. Phys.* **2012**, *111*, 112621. [[CrossRef](#)]
13. Kang, X.D.; Wang, P.; Ma, L.P.; Cheng, H.M. Reversible hydrogen storage in LiBH₄ destabilized by milling with Al. *Appl. Phys. A* **2007**, *89*, 963–966. [[CrossRef](#)]
14. Hansen, B.R.S.; Ravnsbaek, D.B.; Reed, D.; Book, D.; Gundlach, C.; Skibsted, J.; Jensen, T.R. Hydrogen storage capacity loss in a LiBH₄-Al composite. *J. Phys. Chem. C* **2013**, *117*, 7423–7432. [[CrossRef](#)]
15. Gao, J.; Adelmhelm, P.; Verkuijlen, M.H.W.; Rongeat, C.; Herrich, M.; van Bentum, P.J.M.; Gutfleisch, O.; Kentgens, A.P.M.; de Jong, K.P.; de Jongh, P.E. Confinement of NaAlH₄ in nanoporous carbon: Impact on H₂ release, reversibility, and thermodynamics. *J. Phys. Chem. C* **2010**, *114*, 4675–4682. [[CrossRef](#)]
16. Bogdanovic, B.; Brand, R.A.; Marjanovic, A.; Schwickardi, M.; Tolle, J. Metal-doped sodium aluminium hydrides as potential new hydrogen storage materials. *J. Alloys Compd.* **2000**, *302*, 36–58. [[CrossRef](#)]
17. Ravnsbaek, D.B.; Jensen, T.R. Tuning hydrogen storage properties and reactivity: Investigation of the LiBH₄-NaAlH₄ system. *J. Phys. Chem. Solids* **2010**, *71*, 1144–1149. [[CrossRef](#)]
18. Shi, Q.; Yu, X.; Feidenhans'l, R.; Vegge, T. Destabilized LiBH₄-NaAlH₄ mixtures doped with titanium based catalysts. *J. Phys. Chem. C* **2008**, *112*, 18244–18248. [[CrossRef](#)]
19. De Jongh, P.E.; Adelmhelm, P. Nanosizing and nanoconfinement: New strategies towards meeting hydrogen storage goals. *ChemSusChem* **2010**, *3*, 1332–1348. [[CrossRef](#)] [[PubMed](#)]
20. Nielsen, T.K.; Besenbacher, F.; Jensen, T.R. Nanoconfined hydrides for energy storage. *Nanoscale* **2011**, *3*, 2086–2098. [[CrossRef](#)] [[PubMed](#)]
21. Paskevicius, M.; Sheppard, D.A.; Buckley, C.E. Thermodynamic changes in mechanochemically synthesized magnesium hydride nanoparticles. *J. Am. Chem. Soc.* **2010**, *132*, 5077–5083. [[CrossRef](#)] [[PubMed](#)]
22. Nielsen, T.K.; Polanski, M.; Zasada, D.; Javadian, P.; Besenbacher, F.; Bystrycki, J.; Skibsted, J.; Jensen, T.R. Improved hydrogen storage kinetics of nanoconfined NaAlH₄ catalyzed with TiCl₃ nanoparticles. *ACS Nano* **2011**, *5*, 4056–4064. [[CrossRef](#)] [[PubMed](#)]

23. Javadian, P.; Nielsen, T.K.; Ravnsbaek, D.B.; Jepsen, L.H.; Polanski, M.; Plocinski, T.; Kuncze, I.; Besenbacher, F.; Bystrzycki, J.; Jensen, T.R. Scandium functionalized carbon aerogel: Synthesis of nanoparticles and structure of a new ScOCl and properties of NaAlH₄ as a function of pore size. *J. Solid State Chem.* **2015**, *231*, 190–197. [[CrossRef](#)]
24. Nielsen, T.K.; Javadian, P.; Polanski, M.; Besenbacher, F.; Bystrzycki, J.; Jensen, T.R. Nanoconfined NaAlH₄: Determination of distinct prolific effects from pore size, crystallite size, and surface interactions. *J. Phys. Chem. C* **2012**, *116*, 21046–21051. [[CrossRef](#)]
25. Nielsen, T.K.; Bösenberg, U.; Goslawit, R.; Dornheim, M.; Cerenius, Y.; Besenbacher, F.; Jensen, T.R. A reversible nanoconfined chemical reaction. *ACS Nano* **2010**, *4*, 3903–3908. [[CrossRef](#)] [[PubMed](#)]
26. Al-Muhtaseb, S.A.; Ritter, J.A. Preparation and properties of resorcinol-formaldehyde organic and carbon gels. *Adv. Mater.* **2003**, *15*, 101–114. [[CrossRef](#)]
27. Thiangviriyas, S.; Plerdsranoy, P.; Wiset, N.; Javadian, P.; Jensen, T.R.; Utke, R. Hydrogen sorption and reaction mechanisms of nanoconfined 2LiBH₄-NaAlH₄. *J. Alloys Compd* **2015**, *633*, 484–493. [[CrossRef](#)]
28. Jensen, T.R.; Nielsen, T.K.; Filinchuk, Y.; Jorgensen, J.-E.; Cerenius, Y.; Gray, E.M.; Webb, C.J. Versatile *in situ* powder X-ray diffraction cells for solid-gas investigations. *J. Appl. Crystallogr.* **2010**, *43*, 1456–1463. [[CrossRef](#)] [[PubMed](#)]
29. Hansen, B.R.S.; Moller, K.T.; Paskevicius, M.; Dippel, A.C.; Walter, P.; Webb, C.J.; Pistidda, C.; Bergemann, N.; Dornheim, M.; Klassen, T.; *et al.* *In situ* X-ray diffraction environments for high-pressure reactions. *J. Appl. Crystallogr.* **2015**, *48*, 1234–1241. [[CrossRef](#)]
30. Paskevicius, M.; Ley, M.B.; Sheppard, D.A.; Jensen, T.R.; Buckley, C.E. Eutectic melting in metal borohydrides. *Phys. Chem. Chem. Phys.* **2013**, *15*, 19774–19789. [[CrossRef](#)] [[PubMed](#)]
31. Stasinevich, D.; Egorenko, G.; Gnedina, G. Tiermograficzieskoie Issliedovanie Sistemiy Gidridoborat Natrija-Gidrid Natrija. *Dokl. Akad. Nauk SSSR* **1966**, *168*, 610–612.
32. Dilts, J.A.; Ashby, E.C. Study of thermal-decomposition of complex metal hydrides. *Inorg. Chem.* **1972**, *11*, 1230. [[CrossRef](#)]
33. Javadian, P.; Jensen, T.R. Enhanced hydrogen reversibility of nanoconfined LiBH₄-Mg(BH₄)₂. *Int. J. Hydrog. Energy* **2014**, *39*, 9871–9876. [[CrossRef](#)]
34. Javadian, P.; Sheppard, D.A.; Buckley, C.E.; Jensen, T.R. Hydrogen storage properties of nanoconfined LiBH₄-Ca(BH₄)₂. *Nano Energy* **2015**, *11*, 96–103. [[CrossRef](#)]
35. Javadian, P.; Sheppard, D.A.; Buckley, C.E.; Jensen, T.R. Hydrogen storage properties of nanoconfined LiBH₄-NaBH₄. *Int. J. Hydrog. Energy* **2015**, *40*, 14916–14924. [[CrossRef](#)]
36. Ward, P.A.; Teprovich, J.A.; Peters, B.; Wheeler, J.; Compton, R.N.; Zidan, R. Reversible hydrogen storage in a LiBH₄-C₆₀ nanocomposite. *J. Phys. Chem. C* **2013**, *117*, 22569–22575. [[CrossRef](#)]
37. Varin, R.A.; Zbroniec, Z. Decomposition behavior of unmilled and ball milled lithium alanate (LiAlH₄) including long-term storage and moisture effects. *J. Alloys Compd.* **2010**, *504*, 89–101. [[CrossRef](#)]
38. Pitt, M.P.; Paskevicius, M.; Brown, D.H.; Sheppard, D.A.; Buckley, C.E. Thermal stability of Li₂B₁₂H₁₂ and its role in the decomposition of LiBH₄. *J. Am. Chem. Soc.* **2013**, *135*, 6930–6941. [[CrossRef](#)] [[PubMed](#)]
39. Mao, J.F.; Guo, Z.P.; Nevirkovets, I.P.; Liu, H.K.; Dou, S.X. Hydrogen de-/absorption improvement of NaBH₄ catalyzed by titanium-based additives. *J. Phys. Chem. C* **2012**, *116*, 1596–1604. [[CrossRef](#)]
40. Fu, R.; Yoshizawa, N.; Dresselhaus, M.S.; Dresselhaus, G.; Satcher, J.H.; Baumann, T.F. XPS Study of Copper-Doped Carbon Aerogels. *Langmuir* **2002**, *18*, 10100–10104. [[CrossRef](#)]

